A New Hydrazide-Hydrazone Based Schiff Base: Synthesis, DFT Calculations, in Silico Pharmacokinetics and Toxicity, Inhibitory Activity Against Tau Aggregation and SARS-CoV-2 Mpro

Şahin Songül*+

Department of Chemistry, Faculty of Art and Sciences, Ondokuz Mayis University, Samsun, TURKEY

Dege Necmi

Department of Physics, Faculty of Art and Sciences, Ondokuz Mayis University, Samsun, TURKEY

ABSTRACT: *We report here a new imine compound (Schiff base) with a hydrazide-hydrazone moiety, N'-(5-nitro-2-(piperidin-1-yl)benzylidene)benzohydrazide. The present work deals with synthesis, spectral and structural characterization, in silico drug-likeness, target identification, and molecular docking studies of this compound. In this study, structural characterization was performed using complementary spectroscopic techniques, including X-ray, FT-IR, ^{1}H-NMR, and UV-Vis. Surface properties and electronic studies were investigated using the method DFT/B3LYP. Drug-likeness, physicochemical and pharmacokinetic (ADME) properties, toxicity evaluation, and biological target identification were fulfilled using some bioinformatics and cheminformatics web tools. Draggability studies indicated two biological targets for our compound: microtubule-associated protein tau and protease, and docking studies were performed on tau fibrils (5V5C and 3OVL) and Mpro (6LU7) of SARS-CoV-2 accordingly.*

KEYWORDS: *SARS-CoV-2; Tau aggregation; COVID-19; Hydrazide and hydrazone; Schiff Base: Molecular docking.*

INTRODUCTION

Hugo Schiff synthesized Schiff bases for the first time in 1864 [1, 2]. These compounds are also known as azomethines or imines and are represented by the structural formula RHC=NR' [3]. They have found applications in medicine, catalysis, and coordination chemistry as chelating ligands, pharmaceuticals [4], food packaging, dyes, and polymers [5], luminescent probes, analytical chemistry, biological fields [6], chemosensors, and optical materials [7]. The versatile compounds can be synthesized via a condensation reaction between a primary amine and an activated carbonyl group (an aldehyde or ketone) [7-9].

**To whom correspondence should be addressed.*

+ E-mail: songul.sahin@omu.edu.tr

1021-9986/2023/8/2451-2465 15/$/6.05

Hydrazides and hydrazones are a class of organic compounds. They are represented by the general formulas R1(C=O)NHNH2 and R1CH=NNH2, respectively [10]. These compounds are known for their biological activities [11] and pharmaceutical applications in various fields. Some of the biological activities include antibacterial, antitubercular, antifungal, anti-inflammatory, anticonv-ulsant, antiviral, and antiprotozoal effects. Besides, some chemotherapeutic agents, including nitrofurazone, furazolidone, and nitrofurantoin have a hydrazide-hydrazone skeleton [12]. Benzohydrazide, structurally, is a member of the hydrazide family and is known for its antimicrobial activity [13, 14]. Our synthesized compound includes a benzohydrazide skeleton as a primary amine source and an *ortho*-piperidinyl bonded *meta*-nitrobenzylidine (5-nitro-2-(piperidin-1-yl) benzylidine) as an aldehyde source. We preferred benzohydrazide due to the mentioned biological properties above. In 5-nitro-2-(piperidin-1-yl) benzaldehyde, the nitro group deactivates the benzene ring by withdrawing electrons. The electronically deactivated ring increases the electrophilic power of the carbonyl group. The increased electrophilic property results in a much easier nucleophilic attack of benzohydrazide.

In December 2019, a new strain of the coronavirus family emerged in Wuhan, China [15, 16]. Initially, the new strain was named as new coronavirus of 2019 (2019-nCoV), and later, the name of the virus was changed to the severe acute respiratory syndrome coronavirus-2 (SARS-CoV-2). Many therapeutic targets, such as Mpro, PLpro, RdRp, have been reported for both the virus and the host cells to combat the disease [17]. Targeting the main protease or 3-chymotrypsin-like protease (Mpro or 3CLpro) of SARS-CoV-2 is among the strategies to combat the disease, and it plays a vital role in viral replication [17-20].

In the current study, a molecule with Schiff base structure was synthesized. Its molecular structure was identified by spectroscopic techniques. The electronic and surface properties of the title molecule were predicted using the DFT /B3LYP 6-31 G (d, p) method. Some computational drug parameters were studied using chemoinformatics, bioinformatics and docking tools.

EXPERIMENTAL SECTION

Materials

Chemicals: 5-nitro-2-(piperidin-1-yl) benzaldehyde, benzohydrazide, and ethanol were supplied from Sigma Aldrich Company.

Apparatus: Merck TLC plates; CAMAG-UV cabinet; Stuart SMP 30 melting point apparatus, Precisa balance, Heidolph magnetic stirrer

Spectrometer: Perkin-Elmer/FT-IR; Varian Inova 500 MHz/^{1}H-NMR; Thermo Fisher Scientific/UV-Vis; Bruker APEX II QUAZAR /X-ray.

Methods

Experimental

A mixture of the equimolar amounts of 5-nitro-2-(piperidin-1-yl) benzaldehyde (8.0 mg/0.034 mmol) and benzohydrazide (4.6 mg/0.034 mmol) was dissolved in 25 mL of absolute ethanol (Scheme 1). The mixture was refluxed for 22 hours. The reaction progress was monitored by the TLC (hexane/ethyl acetate/ 95:5 for mobile phase). After the reaction was complete, the mixture was filtered by the hot filtration method. The filtrate was slowly cooled down and kept at room temperature to form the crystals. The product was recrystallized from absolute ethanol. The yellow crystals belonging to the product formed two weeks later, and the formed crystals were used for the whole analysis process. Melting point: 222-223 ºC. Yield: 79% (9.48 mg). $C_{19}H_{20}N_4O_3$. Molecular weight: 352.39 g/mol. FT-IR (Attenuated Total Reflectance, ATR), ν/cm^{-1}: 3195 (NH); 3066 (Ar. C-H); 2931, 2849 (Al. C-H); 2823, 2816 (CH=N); 1650 (C=O); 1643 (C=N), 1607, 1601, 1549, 1515, 1504 1493, 1453 (Ar. C=C); 1549, 1327 (NO_2). (Fig. 1). UV-Vis (in EtOH, 5.5 x E-05 M), λmax nm (logε): 359 (4.00); 298 (4.13) (Fig. 2). ^{1}H-NMR (500 MHz, $CDCl_3$) δ: 10.09 (s, 1H, NH); 9.87 (s, 1H, CH=N); 8.86–7.07 (m, 8H, Ar-H); 3.44–2.98 (m, 4H, $2CH_2$); 1.99-1.26 (m, 6H, $3CH_2$) (Fig. 3).

X-ray analysis

The crystal structure of the title compound was solved using SHELXT [21], and the crystal system was refined using SHELXL [22]. All atoms except the hydrogen atoms were refined anisotropically. After the structure solution was completed, the CIF file of the solved structure was written. The CIF file was prepared for further steps using PublCIF [23]. The crystal structure was deposited at CCDC; the deposit number is 2125098.

DFT calculations

The Gaussian 03 package program [24] was used for the DFT [25] calculations. B3LYP 6-31G (d, p) [26] was used for structure optimization and calculation of the frontier molecular orbitals, electrostatic potential map, Mulliken charges, and geometric parameters. We also simulated IR and UV-Vis spectra in the gas phase of the title compound using the B3LYP 6-31G (d, p) level of theory. Mercury [27] was used for molecular graphics and intermolecular interactions.

Docking studies

AutoDock4 and AutoDockTools4 [28] were used for molecular docking experiment. The 3D structure of the proteins was downloaded from the PDB website [29]. Preparation of the ligand and protein structures prior to the docking experiments was performed using AutoDock-Tools. The grid box was placed on the active residues of the protein. The Lamarckian genetic algorithm was used as a search parameter. The output file (DLG) for the most stable complex was converted to the PDB file for further secondary interaction analysis and determination of binding lengths using PLIP [30].

Drug-like nature

Molinspiration and MolTarPred [31] determined possible biological targets of the title compound. SwissADME [32] predicted the ADME, drug-like nature, and some medicinal chemistry properties. ADMETlab-2 [33] was used for ADME and toxicity assessments. Molsoft [34] calculated the drug-likeness score of the title compound and predicted some molecular properties. ProTox-II [35] is a comprehensive tool for toxicity determination and was used for this purpose. SuperCYPsPred [36] evaluated the cytochrome P450s activity of the title compound. The BOILED-Egg method [37] was used to predict gastrointestinal absorption and blood-brain barrier permeability.

RESULTS AND DISCUSSION

Chemistry

A schematic representation for the synthesis of the title compound has been given in Scheme 1. It is a condensation reaction and shows the product forming progress between an active aldehyde (5-nitro-2-(piperidin-1-yl) benzal-dehyde) and a primary amine (benzohydrazide)

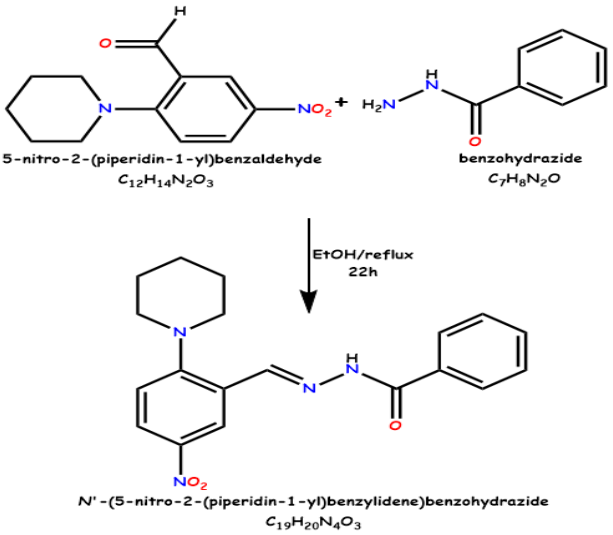

Scheme 1: The synthesis reaction of the title compound

compound. At the end of this reaction, one mole of water is lost and an imine bond forms.

Spectroscopic analysis

We analyzed the molecular structure of the title compound using proton nuclear magnetic resonance, infrared, and electronic absorption spectra. When the functional group region is evaluated from the FT-IR spectrum (Fig. 1), the vibrational band at 3195 cm^{-1} is assigned to the secondary amine, the band at 3195 cm^{-1} is assigned to the aromatic proton, the bands at 2931 and 2849 cm^{-1} are evaluated as aliphatic protons. We assigned the bands at 2823 and 2816 cm^{-1} for azomethine CH vibrations [38]. The carbonyl band is observed at 1650 cm^{-1} [39]. The imine band is observed at 1643 cm^{-1} [40, 41]. The seven peak groups between 1607 and 1453 cm^{-1} are assigned to aromatic double bonds. Asymmetric and symmetric vibrational bands in the nitro group are observed at 1549 and 1327 cm^{-1}, respectively [42]. The FT-IR spectrum of the title compound (Fig. S1) in the gas phase also agrees with the experimental spectrum with minor deviations. The electronic absorption spectra of the title compound in ethanol (experimental) and in the gas phase (calculated) using the B3LYP/6-31G (d, p) basis set are shown in Fig. 1. In the experimental spectrum, two absorption maxima are observed at 298 and 359 nm, which are due to $\pi \rightarrow \pi^*$ and $n \rightarrow \pi^*$ charge transitions [43] in the structure, respectively. On the other hand, the theoretical spectrum shows only one absorption maximum at 338 nm, which is due to the absence of solvent effects, similar to

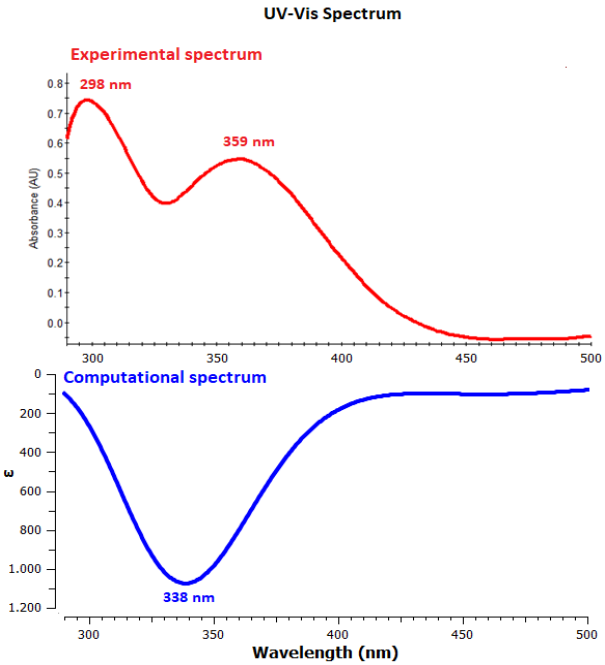

Fig. 1: Computational and experimental UV-Vis spectra of title compound

another study [44]. In the title structure, we can divide all protons into four parts: aliphatic protons, aromatic protons, imine, and amine protons. Examining the ^{1}H-NMR spectrum in Fig. S2, the resonance peaks of the aliphatic protons in the piperidine ring range from 3.44 to 1.26 ppm, in which the protons near the nitrogen are in the downfield and far protons are in the upfield. The resonance peaks of the aromatic protons range from 8.86 to 7.07 ppm. The resonance peak of the imine proton is observed at 9.87 ppm. The secondary amine proton is observed at 10.09 ppm.

Crystallographic, structural, and geometrical properties

The crystallographic data gave the molecular structure shown in Fig. 2, which is expected from the condensation reaction of the aldehyde and amine reactants. The main features of the crystal molecule are a monoclinic crystal system, the space group P21/c, and the formation of the four monomeric units of the unit cell. Structurally, this compound consists of two aromatic rings, one aliphatic ring (piperidinyl), one nitro substituent, one carbonyl group, one secondary amine, and one imine. Fig. 2A shows a section through the crystal packing. Fig. 2B shows the numbered shape of the molecule and the bond lengths that form the secondary interaction forces. Fig. 2C shows the molecular structure with the thermal ellipsoid plots at a 50% probability level. Three hydrogen bonds are observed in the crystal structure, all of which are belonging oxygen-hydrogen interactions. The bond lengths for these bonds change between 2.243 to 2.7076 Å. The CIF file of the title crystal was deposited in the CCDC data centre with the deposit code 2125098. For the crystal structure, the detailed crystal parameters, bond lengths, bond angles and torsion angles were listed in Table S1, S2, S3 and S4, respectively. The selected five bond lengths and bond angles are: N1—O2: 1.223, C1—C2: 1.373, C8—C9: 1.512, C13—O3: 1.224, C7—N3: 1.275 Å; C1—C2—C3: 121.43 (18)^{o}, O1—N1—O2: 122.7 (2)^{o}, C8—C9—C10: 112.4 (2)^{o}, C7—N3—N5: 117.16 (15)^{o}, C13—N5—N3: 117.64 (15)^{o}.

Molecular electrostatic potential (MEP) and Mulliken atomic charges

MEP is a 3D pictorial method to see the distribution of electron density and the net electrostatic effect in the molecules. It is related to the partial charge, electronegativity, and chemical reactivity [45]. The MEP is a useful technique for several assessments, including determining electrophilic and nucleophilic positions [46, 47], predicting reactivity, evaluating the hydrogen bonding interactions, and the biological recognition process [48]. A MEP surface is colored by various colors changing from red to blue. The red, green, and blue colors represent the most negative electrostatic potential zone, zero electrostatic potential, and most positive electrostatic potential, respectively [49]. Because of the high electron density of the red regions, they are nucleophilic reactive sites and open to interactions with electrophilic species. Because of the high electropositive nature of the blue regions, they are electrophilic reactive sites and suitable places for nucleophilic attacks. To predict the electrophilic and nucleophilic positions of the title molecule, we calculated the MEP map in the gas phase at the B3LYP/6-31G (d, p) level of theory. The calculated MEP of the title molecule is displayed in Fig. 3. The MEP is composed of red, dark blue, yellow, cyan, and green regions. Our compound has electrophilic and nucleophilic positions according to the explanations mentioned above. These positions have been placed on the H5 atom (electrophilic place); O1, O2, and O3 atoms (nucleophilic places). The other positions are colored in yellow and cyan, and

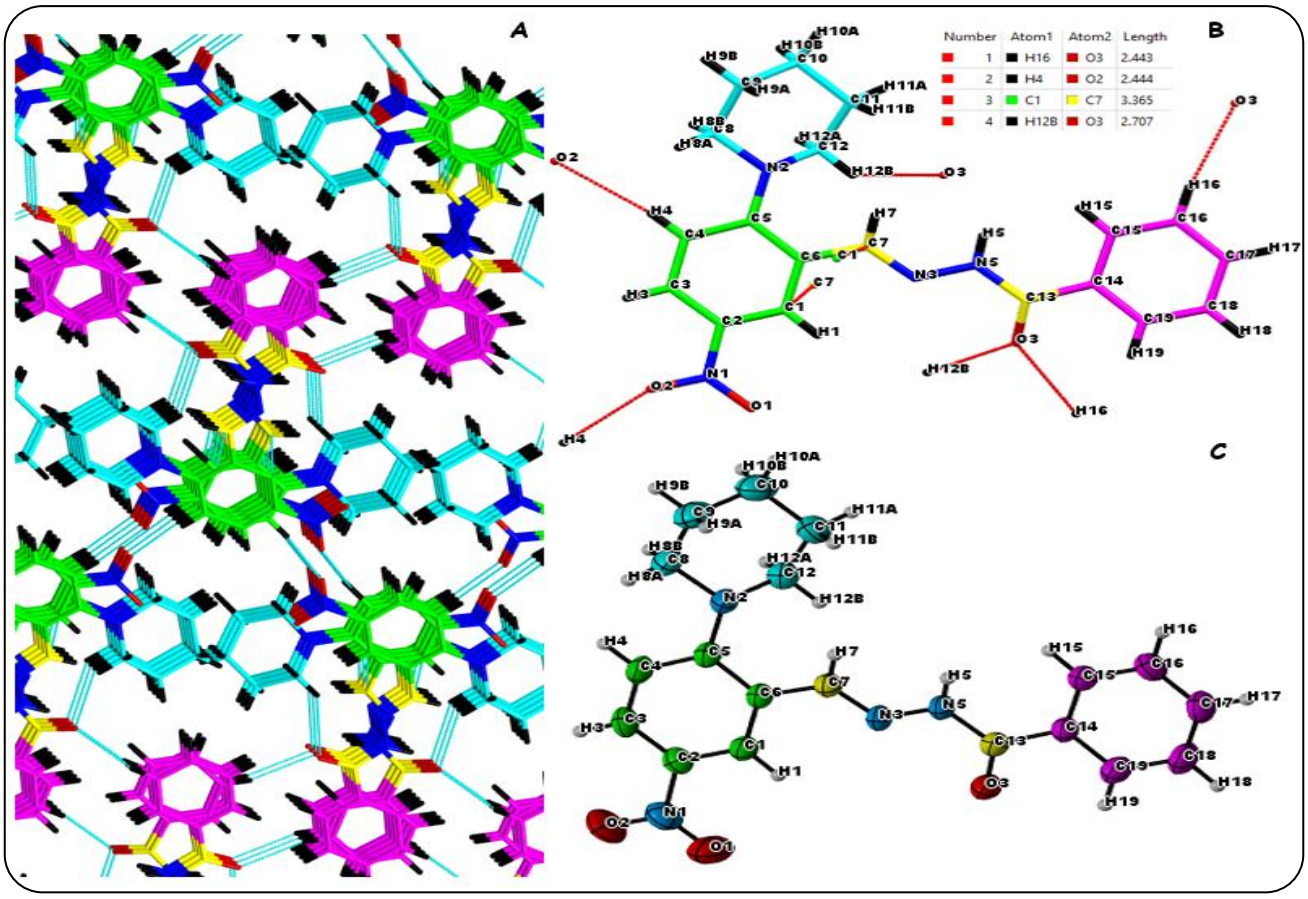

Fig. 2: A view of crystal packing of the title molecule (A). Molecular structure of the title molecule with the atom numbering scheme, and the list and bond lengths of hydrogen bonds, and vdW forces for the secondary interactions in the crystal packing (B). Thermal ellipsoid diagram (50% probability level) of the title molecule (C)

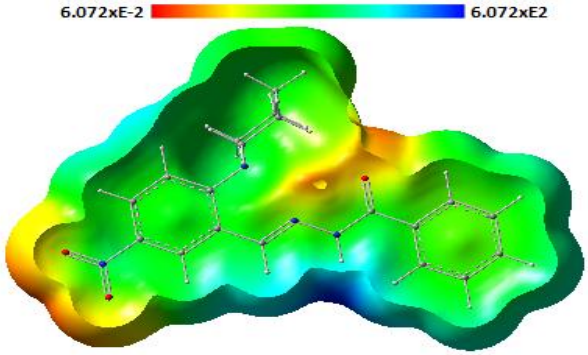

Fig. 3: Molecular electrostatic potential map for the title compound

the attack possibility to these regions is lower than dark blue and dark red regions. The green regions are zero electrostatic potential zones. Fig. S3 (b) and (c) show the Mulliken atomic charges of the title molecule as the colors and quantitative charge values. The top-four positive and negative charged atoms in the title molecule are +0.592 (C13), +0.373 (N1), +0.268 (C2), 0.250 (H5); -0.494 (O3), -0.436 (N2), -0.435 (N5), and -0.400 (O1). The most opposite characterized charges are on the atoms of the carbonyl group because of the high polarizable nature of the carbonyl groups.

Molecular orbital analysis and global reactivity descriptors

Frontier Molecular Orbitals (FMOs), also known as the Highest Occupied Molecular Orbital (HOMO) and the Lowest Unoccupied Molecular Orbital (LUMO), are the most critical orbitals in a molecule. The HOMO is an electron donor orbital, while the LUMO is an electron acceptor orbital. The energies of these orbitals are directly related to the ionization potential and electron affinity. The frontier orbital gap is defined as energy difference between HOMO and LUMO. The HOMO/LUMO gap or the energy gap determines molecular stability, reactivity, polarizability [50-52], softness, and hardness. While

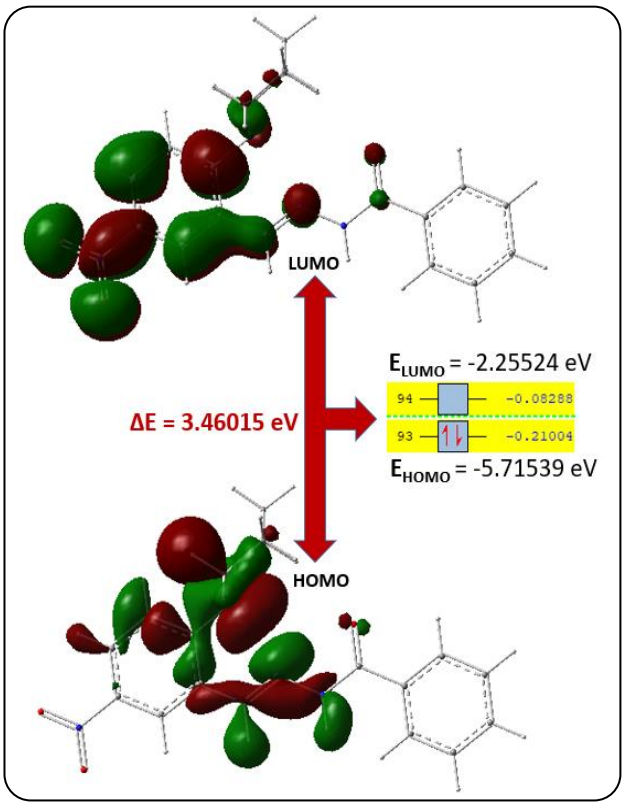

Fig. 4: Frontier orbitals (HOMO and LUMO) and their energy values for the title molecule

a large energy gap indicates hardness of a molecule, a small energy gap indicates softness [51]. The UV-Vis spectral properties of compounds can be explained using these molecular orbitals The global reactivity parameters of a molecule can also be calculated using the energies of the HOMO and LUMO orbitals. We calculated these parameters of the title compound according to the equations given in the study [53]. The FMOs of the title molecule were calculated in the gas phase at the B3LYP/6-31 G (d, p) level of theory. The pictorial representation of the HOMO and the LUMO orbitals along with the energy gap of the title molecule are available in Fig. 4. From Fig. 4, it can be seen that the HOMO orbitals are localized throughout the N5-N2 bond line, while the LUMO orbitals are localized throughout the N3-NO_2 bond line. This difference is evidence of charge transfer between HOMO and LUMO orbitals, and the presence of UV-Vis absorption bands (Fig. 1) in the title molecule. The global reactivity parameters of the title molecule are listed in Table 1. As shown in Fig. 4 and Table 1, the calculated energies of HOMO, LUMO, and the energy gap (ΔE) are -5.715 eV, -2.255 eV, and 3.460 eV, respectively. The energy gap value for the title molecule was calculated to be the lowest among our similar studies [49, 54, 55]. According to the calculated energies and global reactivity descriptors, the title molecule with the small energy gap value is a soft, chemically, and kinetically unstable molecule. The polarizability and intramolecular charge transfer between HOMO and LUMO orbitals are easy. Since the value of the energy gap is lower than that of the reference molecule urea (ΔE=6.7063 eV) [56], the studied molecule can be theoretically considered as a good NLO-active material.

Table 1: The calculated global reactivity descriptors

Parameters	Values (eV)
E_{HOMO}	-5.71539
E_{LUMO}	-2.25524
Energy band gap ($\Delta E=E_{LUMO}-E_{HOMO}$)	3.46015
Ionization potential ($I=-E_{HOMO}$)	5.71539
Electron affinity ($A=-E_{LUMO}$)	2.25524
Chemical hardness ($\eta=(I-A)/2$)	1.73007
Chemical softness ($\sigma=1/2\eta$)	0.28900
Electronegativity ($\chi=(I+A)/2$)	3.98531
Chemical potential ($\mu=-(I+A)/2$)	-3.98531
Electrophilicity index ($\omega=\mu^2/2\eta$)	4.59020
Maximum charge transfer index ($\Delta N_{max}=-\mu/\eta$)	2.30355

Druggability and docking studies

This section is related to the docking experiments and aims to determine the possible biological targets of the title molecule. One of the tools used for this purpose is MolTarPred. This prediction tool uses Tonimato similarities between the query compound and 607,669 ChEMBL compounds with ten micromoles or less activity for 4,553 targets. We have listed the targets predicted by MolTarPred in Table S5. Molinspiration is another web tool that indicates our molecule as a protease inhibitor (Fig. S4). Based on the results in Table S5 and Fig. S4, we selected two biological targets, microtubule-associated protein tau and main protease of SARS-CoV-2 (Mpro), for docking studies. The docking studies determined the inhibitory activities of the query compound and the reference molecules against Mpro of SARS-CoV-2 and the aggregation-forming segments of tau protein (275-VQIINK-280 and 306-VQIVYK-311).

Docking experiments were performed using AutoDock 4.2 and AutoDockTools 4.2. The grid box was placed on the active sites of Mpro for SARS-CoV-2 (PDB ID: 6LU7)

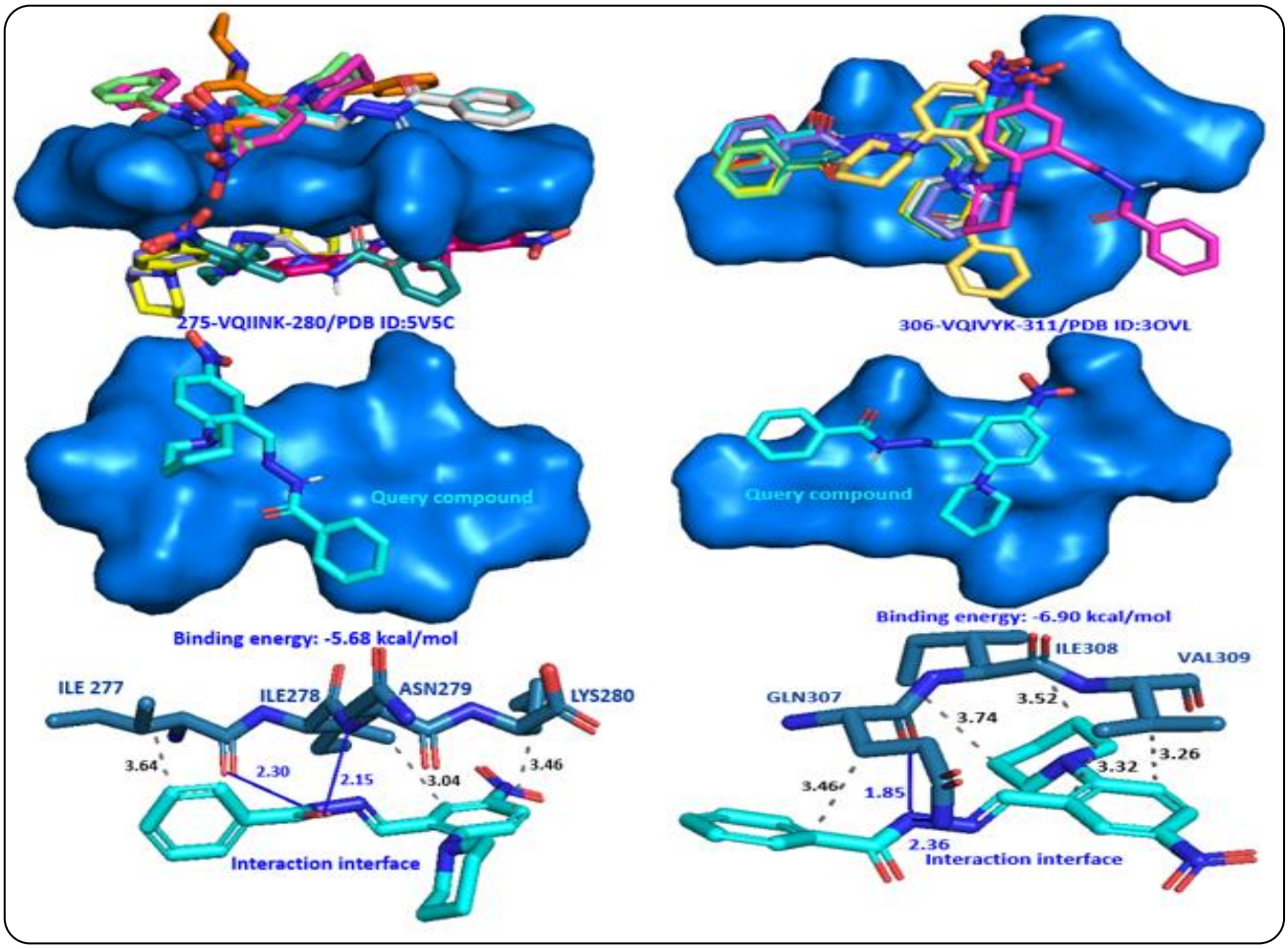

Fig. 5: The top ten conformations were produced from docking experiments of the query compound with aggregation-forming segments of tau (VQIINK: top-left; VQIVYK: top-right). The most stable conformations of the query compound with VQIINK (middle-left) and VQIVYK (middle-right). Interaction interfaces of the query compound with VQIINK (bottom-left) and VQIVYK (bottom-right) (cyan: query compound; Prussian blue: interacting residues, blue line/s: hydrogen bond/s; grey dots: vdW interactions)

and the entire sequence segments of tau, which are responsible for aggregation (PDB IDs: 5V5C and 3OVL). A Lamarckian genetic algorithm was used for the docking experiments. Macromolecules were prepared by adding Kollman charges, removing water molecules and nonpolar hydrogens, and merging polar hydrogens before the docking process. Each docking experiment yielded ten docking poses, which were then ranked according to their energy. The complex with the lowest energy was selected, and its binding energy was compared with the reference molecules. Fig. S5 shows the aggregation-forming segments (275-VQIINK-280 and 306-VQIVYK-311) of the tau protein and their amino acid sequence. Fig. 5 shows the generated conformations of the title molecule (top) on the tau segments, the complexes with the lowest energies (middle), and the explanations of the interaction interfaces between the query molecule and the residues for the most stable conformations (bottom). Fig. 6 shows the generated conformations in the active sites of Mpro, the most stable conformation and its binding energy, and finally, the interaction diagram between the active sites and the query compound. The comprehensive quantitative results of the docking experiments for both the query compound and the reference molecules are shown in Table. S6.

For the tau segments, the docking scores of the query compound were calculated to be -5.68 and -6.90 kcal/mol for VQIINK and VQIVYK, respectively. The reference molecule EGCG has a binding energy of -3.90 and -5.00 kcal/mol. The inhibitory effect of the query compound for tau segments is higher than that of the reference molecule

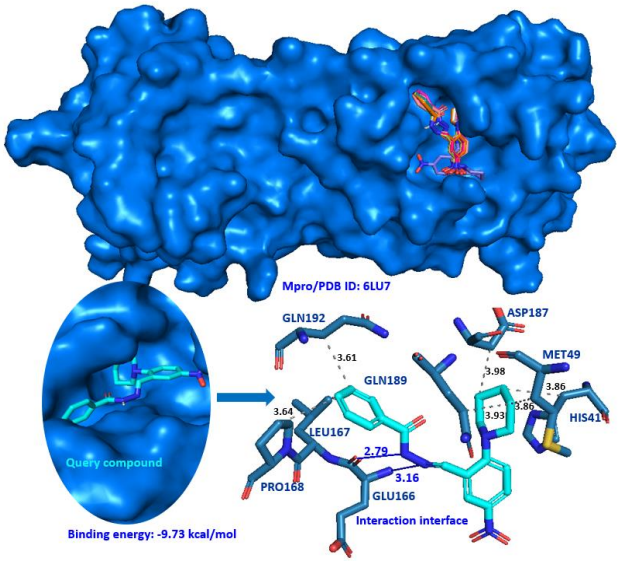

Fig. 6: The ten generated conformations of the query compound in the active pockets of Mpro (top); the most stable conformation of the query compound in the active site (bottom-left); Interaction interface for the most stable complex between the query compound and the active pockets of Mpro (bottom-right, cyan: query compound; Prussian blue: interacting residues, blue lines: hydrogen bonds; grey dots: VdW interactions)

EGCG. The ligand efficiencies of the query compound on VQIINK and VQIVYK were calculated to be -0.22 and -0.27, and the inhibition constants are 68.98 μM and 8.79 μM, respectively.

For the Mpro of SARS-CoV-2, the binding energies of the query compound and reference N3 (native ligand) were calculated to be -9.73 and -7.11 kcal/mol, respectively. The inhibitory activity of the query compound for Mpro is also higher than that of the native inhibitor N3. The query compound's ligand efficiency and inhibitor constant were calculated to be -0.37 and 74.0 nM, respectively.

Druglike nature, physicochemical properties, medicinal chemistry

Pharmacokinetics is a branch of the drug development process. It investigates the transformation process (absorption, distribution, metabolism, and excretion) of a drug, new chemical substance, or compound in the body [57]. In the current section, we investigated some physicochemical and pharmacokinetic properties, solubility, drug-likeness, and medicinal chemistry properties for the title molecule. We carried out the investigations *via* free in silico web tools, including SwissADME, ADMETlab 2.0, and Molsoft. Table S7, Table 2, and Fig. S6 show the prediction results for SwissADME, ADMETlab 2.0, and Molsoft, respectively. SwissADME and ADMEDlab 2.0 determine the ideal region with a polygon that offers a suitable drug space and the position of query compound in this space regarding physicochemical descriptors. As can be seen from the hexagon in Table S7, there is no deviation from the suitable domain regarding the physicochemical properties of the title molecule. As for ADMETlab 2.0 results, it investigates many physicochemical parameters, including molecular weight (MW), the logarithm of n-octanol/water partition coefficient (logP), the logarithm of n-octanol/water partition coefficient at pH 7.4 (logD), Topological Polar Surface Area (TPSA), formal charge (fChar), the logarithm of aqueous solubility (logS), number of heteroatoms (nHet), number of rigid bonds (nRig), number of atoms biggest ring (MaxRing), number of hydrogen bond acceptor and donors (nHA and nHD), and so on. Two physicochemical descriptors signal the out-of-domain: logP and logD. The ideal values for logP and logD change from 0 to 3 mol/L, 1 to 3 mol/L, respectively. For our compound, the two parameters were calculated to be 4.682 and 3. 818 mol/L, respectively. The title molecule is compatible with the known drug-likeness rules, such as Lipinski, Ghose, Weber, Egan, Muegge, and Pfizer. According to the Molsoft software, the drug-likeness score of the title molecule is -0.42 (red line in Fig. S6). This value is almost the median between drug and non-drug compounds. Hence, it is difficult to say whether we can regard the title molecule as a drug candidate.

Cytochrome P450 activity analysis

Cytochrome P450 enzymes (P450s) is a family of isoenzymes responsible for the biotransformation of xenobiotics, including drug compounds and exogenous chemicals. Because of their role in drug metabolism and drug-drug interactions (DDIs), CYPs activity is a critical issue for the pharmaceutical industry. CYPs-active drugs can act as inhibitors, inducers, or substrates for a specific CYP enzymatic pathway [58]. The major isoforms are CYP1A2, CYP2C9, CYP2C19, CYP2D6, and CYP3A4 (5CYPs) [59, 60], and they are responsible for over 80% of the metabolism of clinically approved drugs [61]. Here, we report the results of CYPs activity for the molecule of interest. We obtained these results using the SuperCYPsPred prediction algorithm and inputting the canonical SMILES

Table 2: Physicochemical, medicinal, and ADME properties of the title molecule

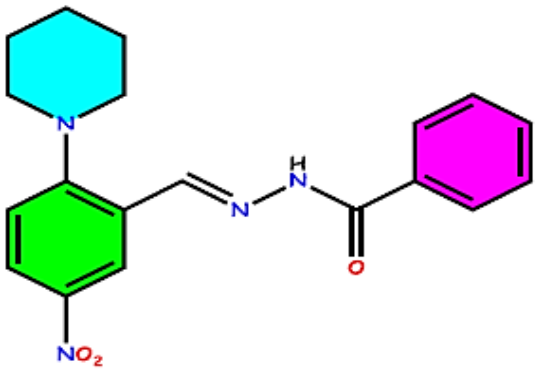

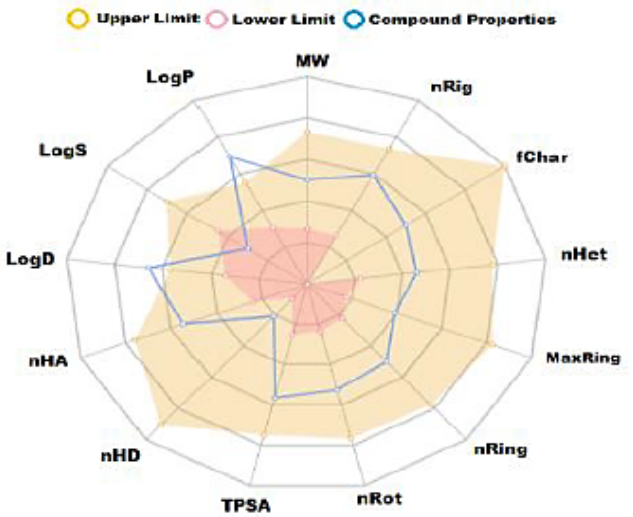

Physicochemical Property		
Molecular Weight (MW)	352.150	
Volume	358.140	
Density	0.983	
nHA	7	
nHA	1	
nRot	6	
nRing	3	
MaxRing	6	
nHet	7	
fChar	0	
nRig	21	
Flexibility	0.286	
Stereo Centers	0	
TPSA	87.840	
logS	-6.724	
logP	4.682	
logD	3.818	
Absorption		
Caco-2 Permeability	-4.607	●
MDCK Permeability	0.00013	●
Pgp-inhibitor	---	●
Pgp-substrate	---	●
HIA	---	●
F20%	---	●
F30%	-	●
Excretion		
CL	4.242	●
T1/2	0.149	

Medicinal Chemistry		
QED	0.508	●
SAscore	2.092	●
Fsp3	0.263	●
MCE-18	38.667	●
NPscore	-1.881	
Lipinski Rule	Accepted	●
Pfizer Rule	Accepted	●
GSK Rule	Rejected	●
Golden Triangle	Accepted	●
PAINS	0 alert(s)	
ALARM NMR Rule	3 alert(s)	
BMS Rule	0 alert(s)	
Chelator Rule	0 alert(s)	
Distribution		
PPB	99.064%	●
VD	0.767	●
BBB Penetration	--	●
Fu	0.497%	●
Metabolism		
CYP1A2 inhibitor	++	
CYP1A2 substrate	--	
CYP2C19 inhibitor	++	
CYP2C19 substrate	--	
CYP2C9 inhibitor	++	
CYP2C9 substrate	++	
CYP2D6 inhibitor	-	
CYP2D6 substrate	+	
CYP3A4 inhibitor	++	
CYP3A4 substrate	--	

Tip: For the classification endpoints , the prediction probability values are transformed into six symbols: 0-0.1(---), 0.1-0.3(--), 0.3-0.5(-), 0.5-0.7(+), 0.7-0.9(++), and 0.9-1.0(+++).

Excellent ●
Medium ●
Poor ●

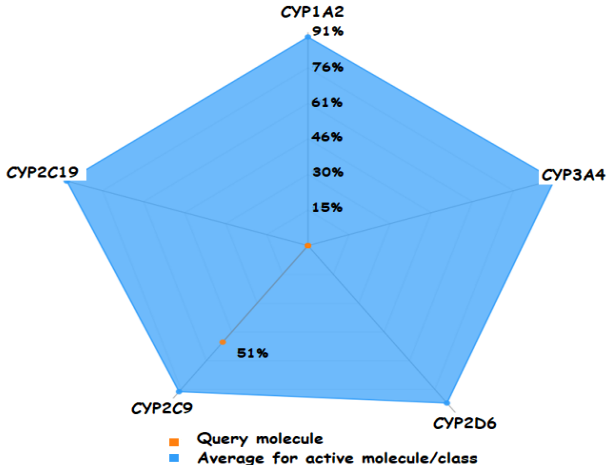

Fig. 7: 5CYPs activity results calculated by SuperCYPsPred of the query compound

code of the molecule of interest. The prediction results by MACCS and MORGAN fingerprints are shown in Table 3. The MACCS fingerprints showed the molecule of interest as "active" for the CYP2C9 isoenzyme. The probability strength of our molecule for CYP2C9 activity was 51% (Fig. 7, MACCS model). In addition, the other two in silico tools, ADMETlab 2.0 and SwissADME, calculated the CYP activity of the thematic compound on the mentioned 5 CYPs (Table 2 and Table S7). SwissADME found that the title molecule was an inhibitor of 5 CYPs, except for CYP1A2. ADMETlab evaluated the input molecule's inhibitor and substrate activity and calculated it as an inhibitor for 5CYPs except for CYP2D6. The title molecule is not a strong substrate for 5 CYPs. Three web tools have reported different results for CYPs activity using different algorithms, and the results are not very similar. However, all three agreed that the title compound is active for at least one or more CYPs within the isoenzymes studied. In summary, the title molecule cannot include in a safe profile concerning CYPs activity. It may cause drug-drug interactions or an increased or decreased pharmacokinetic profile in the body.

Toxicity analysis

Here we present in silico toxicity assessments for the title molecule. Toxicity predictions were performed using the online web tools ADMETlab 2.0 and ProTox- II. The results predicted by ProTox- II have been given in Table S8, and a radar plot model regarding these results is in Fig. S7. The results obtained from ADMETlab 2.0 have been shown in Table S9. ProTox- II showed that the compound

Table 3: Cytochrome activity prediction results for the title molecule

Cytochrome Activity Prediction Table

Cytochrome	Fingerprint	Prediction	Probability
CYP1A2	maccs	Inactive	0.851
CYP2C19	maccs	Inactive	0.741
CYP2C9	maccs	Active	0.509
CYP2D6	maccs	Inactive	0.583
CYP3A4	maccs	Inactive	0.595
CYP1A2	morgan	Inactive	0.77
CYP2C19	morgan	Inactive	0.767
CYP2C9	morgan	Inactive	0.677
CYP2D6	morgan	Inactive	0.584
CYP3A4	morgan	Inactive	0.685

Probability strength: high, medium, low

is mutagenic and carcinogenic. The probability level of mutagenicity and carcinogenicity is 78% and 66%, respectively. ADMETlab 2.0 evaluated the toxicity properties of the query compound and ranked the results as excellent (green), moderate (yellow), and poor (red). Green means no toxicity, and red means that high toxicity is suspected. In this context, the query compound needs evaluation regarding toxicity in the following matters: DILI, AMES toxicity, skin sensitization, eye irritation, and respiratory toxicity. Drug-Induced Liver Injury (DILI) is common, and almost any drug can cause liver disease. However, most DILI cases improve after drug treatment [62]. The AMES assay is an experimental method for determining mutagenicity. Computationally, it can be predicted by a Quantitative Structure-Activity Relationship (QSAR) using accumulated experimental assay data [63]. The query compound has been predicted as both mutagenic and carcinogenic. In Section 3.3, the electrophilic nature of the query compound has been described in detail using the MEP map. Our toxicity results are consistent with the theory that electrophilic structures can be mutagenic and carcinogenic [64]. The results (Table S9) within twelve Tox21 assays [65, 66] showed that the query compound is toxic (++ and +++) for five signaling pathways: aryl hydrocarbon receptor (NR -AhR), nuclear factor (erythroid-derived 2)-like2/antioxidant responsive element (SR-ARE), ATAD5, mitochondrial membrane potential (SR-MMP), and p53.

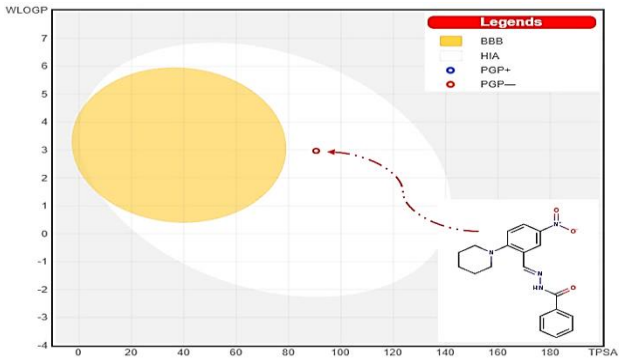

Fig. 8. BOILED-Egg model of the title molecule for the prediction of BBB permeability and GI absorption

Gastrointestinal absorption and brain penetration

In this section, gastrointestinal absorption and blood-brain barrier permeability for the molecule of interest were studied. For this purpose, the BOILED-Egg model developed by *Daina* and Zoete [37] was used. This model calculates the lipophilicity and polarity of small molecules, and a BOILED-Egg model is constructed, as shown in Fig. 8. The egg yolk represents good permeability to the brain, while the white ellipse represents good absorption in the human intestine. These yellow and white areas are not mutually exclusive. The colored small circle in the model shows the zone of the drug or molecule under study and offers information about the BBB and GI absorption of the molecule. Our molecule has settled in the white region. So, the human gastrointestinal tract can absorb the studied substance, but the permeability of the BBB is not good because the colored circle does not fall in the yolk region.

CONCLUSIONS

In conclude, our results show that: the new Schiff base containing a hydrazine-hydrazone framework crystallizes in the monoclinic system, has space group P21/c and deposits four monomeric molecules in the unit cell (Z=4). The most oppositely charged atoms in the structure are C13 (+0.592) in the carbonyl group and O3 (-0.494) in the nitro group. The compound has both electrophilic and nucleophilic sites. Therefore, it is a reactive compound and open to electrophilic and nucleophilic attack by other species. The energy gap value was found to be 3.460 eV. This low value makes it a soft, kinetically and chemically unstable, polarizable material. The free binding energy with the tau segments, VQIINK and VQIVYK, was calculated to be -5.68 and -6.90 kcal/mol, respectively. These values are higher than those of the reference EGCG (-3.90 and -5.00 kcal/mol). The free binding energy for Mrpo complex was calculated to be -9.73 kcal/mol, and this value is higher than that of the reference inhibitor N3 (-7.11 kcal/mol). Therefore, the inhibitory activity of the title compound for tau and Mpro is better than that of the reference molecules. The title compound has good physicochemical descriptors in the corresponding domains of the bioinformatics tools, SwissADME and ADMETlab, except logP and logD. There are no violations of drug-likeness rules. The drug-likeness score of the compound was calculated to be -0.42. The value is a median between drugs and non-drugs. The metabolization rate of the compound may be affected by 4CYPs, as it is active for CYP 2C19, 2C9, 3A4 and 2D6 according to SuperCYPsPred and SwissADME. Unfortunately, the compound can be mutagenic and carcinogenic. The prediction results for BBB penetration and gastrointestinal absorption have shown negative and positive results, respectively.

Received : Aug. 08, 2022 ; Accepted : Dec. 19, 2022

REFERENCES

[1] Hassan S., Abdullah M., Synthesis, Spectroscopic Study and Biological Activity of Some New Heterocyclic Compounds Derived from Sulfadiazine, *ZANCO Journal of Pure and Applied Sciences*, **31(6)**: 92-109 (2019**)**.

[2] Hassan S., Abdullah M. Aziz D., Synthesis, in Vitro Antimicrobial Assay and Molecular Docking Studies of some New Symmetrical Bis-Schiff Bases and Their 2-Azetidinones, *Scientific Journal of Pure and Applied Sciences*, **33**: 34-50 (2021**)**.

[3] Hussain Z., Yousif E., Ahmed A. Altaie A., Synthesis and Characterization of Schiff's Bases of Sulfamethoxazole, *Organic and Medicinal Chemistry Letters*, **4(1)**: 1-1 (2014**)**.

[4] Menati S., Azadbakht R., Rudbari H.A. Bruno G., Synthesis and Characterization of Four New Azo-Schiff Base and Their Nickel(II) Complexes, *Polyhedron*, **205**: 115296 (2021**)**.

[5] More M.S., Joshi P.G., Mishra Y.K., Khanna P.K., Metal Complexes Driven from Schiff Bases and Semicarbazones for Biomedical and Allied Applications: A Review, *Materials Today Chemistry*, **14**: 100195 (2019**)**.

[6] Talebi A., Salehi M., Khaleghian A., Synthesis, Characterization, Electrochemical Behavior, Molecular Simulation Studies and in Vitro Toxicity Assessment of New Metal Schiff Base Complexes Derived from 3-Methoxy-2-Hydroxy-Benzaldehyde and Allylamine, *Journal of Molecular Structure*, **1246**: 131076 (2021**)**.

[7] Murašková V., Eigner V., Dušek M., Sedmidubský D., Iron(III) and Cobalt(Iii) Complexes with Pentadentate Pyridoxal Schiff Base Ligand – Structure, Spectral, Electrochemical, Magnetic Properties and DFT Calculations, *Polyhedron*, **197**: 115019 (2021**)**.

[8] Li Z., Jiang Y., Guengerich F.P., Ma L., Li S., Zhang W., Engineering Cytochrome P450 Enzyme Systems for Biomedical and Biotechnological Applications, *Journal of Biological Chemistry*, **295(3)**: 833-849 (2020**)**.

[9] Kırca B.K., Kaştaş Ç.A.m Ersanlı C.C., Molecular and Electronic Structures of Two New Schiff Base Compounds: (E)-2-Bromo-6-[(2-Bromo-4-Methylphenylimino) Methyl]-4-Chlorophenol and (E)-2-Bromo-6-[(4-Bromo-3-Methylphenylimino) Methyl]-4-Chlorophenol, *Journal of Molecular Structure*, **1241**: 130643 (2021**)**.

[10] Boulebd H., Zine Y., Khodja I.A., Mermer A., Demir A., Debache A., Synthesis and Radical Scavenging Activity of New Phenolic Hydrazone/Hydrazide Derivatives: Experimental and Theoretical Studies, *Journal of Molecular Structure*, **1249**: 131546 (2022**)**.

[11] Hassan S., Abdullah M., Aziz D., Synthesis of New Series Bis-3-Chloro-β-Lactam Derivatives from Symmetrical Bis-Schiff Bases as Effective Antimicrobial Agents with Molecular Docking Studies, *Science Journal of University of Zakho*, **9**: 128-137 (2021**)**.

[12] Popiołek Ł., Hydrazide–hydrazones as Potential Antimicrobial Agents: Overview of the Literature Since 2010, *Medicinal Chemistry Research*, **26(2)**: 287-301 (2017**)**.

[13] Yele V., Mohammed A.A., Wadhwani, A.D., Synthesis and Evaluation of Aryl/Heteroaryl Benzohydrazide and Phenylacetamide Derivatives as Broad-Spectrum Antibacterial Agents, *Chemistry Select*, **5(34)**: 10581-10587 (2020**)**.

[14] Lalavani N.H., Gandhi H.R., Bhensdadia, K.A., Patel R.K. Baluja S.H., Synthesis Pharmacokinetic and Molecular Docking studies of New Benzohydrazide Derivatives Possessing Anti-Tubercular Activity Against Mycobacterium Tuberculosis H37Rv, *Journal of Molecular Structure*, **1250**: 131884 (2022**)**.

[15] Farahani M., Niknam Z., Mohammadi Amirabad L., Amiri-Dashatan N., Koushki M., Nemati M., Danesh Pouya, F., Rezaei-Tavirani M., Rasmi Y., Tayebi L., Molecular Pathways Involved in COVID-19 and Potential Pathway-Based Therapeutic Targets, *Biomedicine & Pharmacotherapy*, **145**: 112420 (2022**)**.

[16] Bhat A., Dongre R., Patil R., Abdullah M., Hassan S., Inventum Biologicum SARS-CoV-2 and Diabetes Mellitus (DM): *A Comprehensive Review*, *International Journal of Biological Research*, **2**: 87-93 (2022**)**.

[17] Zhou Y.-W., Xie Y., Tang L.-S., Pu D., Zhu Y.-J., Liu J.-Y. Ma X.-L., Therapeutic Targets and Interventional Strategies in COVID-19: Mechanisms and Clinical Studies, *Signal Transduction and Targeted Therapy*, **6(1)**: 317 (2021**)**.

[18] Qia, Z., Wei N., Jin L., Zhang H., Luo J., Zhang Y. Wang K., The Mpro Structure-Based Modifications of Ebselen Derivatives for Improved Antiviral Activity Against SARS-CoV-2 Virus, *Bioorganic Chemistry*, **117**: 105455 (2021**)**.

[19] Jena N.R., Drug targets, Mechanisms of Drug Action, and Therapeutics Against SARS-CoV-2, *Chemical Physics Impact*, **2**: 100011 (2021**)**.

[20] Oubahmane M., Hdoufane I., Bjij I., Jerves C., Villemin D. Cherqaoui D., COVID-19: In silico Identification of Potent A-Ketoamide Inhibitors Targeting the Main Protease of the SARS-CoV-2, *Journal of Molecular Structure*, **1244**: 130897 (2021**)**.

[21] Sheldrick G.M., SHELXT - Integrated Space-Group and Crystal-Structure Determination, *Acta Crystallographica Section A: Foundations of Crystallography*, **71(1)**: 3-8 (2015**)**.

[22] Sheldrick G.M., Crystal Structure Refinement with SHELXL, *Acta Crystallographica Section C: Structural Chemistry*, **71(1)**: 3-8 (2015**)**.

[23] Westrip S.P., PublCIF: Software for Editing, Validating and Formatting Crystallographic Information Files, *Journal of Applied Crystallography*, **43(4)**: 920-925 (2010**)**.

[24] Frisch M., Trucks G., Schlegel H.B., Scuseria G.E., Robb M.A., Cheeseman J.R., Scalmani G., Barone V., Mennucci B. Petersson G., Gaussian 09, Revision d. 01, Gaussian, Inc., *Wallingford CT*, **201** (2009**)**.

[25] Parr R.G., "Density Functional Theory of Atoms and Molecules", Springer, (1980).

[26] Becke A.D., Density-Functional Thermochemistry. III. The Role of Exact Exchange, *The Journal of Chemical Physics*, **98(7)**: 5648-5652 (1993**)**.

[27] Macrae C.F., Edgington P.R., McCabe P., Pidcock E., Shields G.P., Taylor R., Towler M., Van De Streek J., Mercury: Visualization and Analysis of Crystal Structures, *Journal of Applied Crystallography*, **39(3)**: 453-457 (2006**)**.

[28] Morris G.M., Huey R., Lindstrom W., Sanner M.F., Belew R.K., Goodsell D.S., Olson A.J., AutoDock4 and AutoDockTools4: Automated Docking with Selective Receptor Flexibility, *Journal of Computational Chemistry*, **30(16)**: 2785-2791 (2009**)**.

[29] Berman H.M., Westbrook J., Feng Z., Gilliland G., Bhat T.N., Weissig H., Shindyalov I.N. Bourne P.E., The Protein Data Bank, *Nucleic Acids Research*, **28(1)**: 235-242 (2000**)**.

[30] Salentin S., Schreiber S., Haupt V.J., Adasme M.F. Schroeder M., PLIP: Fully Automated Protein–Ligand interaction Profiler, *Nucleic Acids Research*, **43(W1)**: W443-W447 (2015**)**.

[31] Peón A., Li H., Ghislat G., Leung K.S., Wong M.H., Lu G., Ballester P.J., MolTarPred: A Web Tool for Comprehensive Target Prediction with Reliability Estimation, *Chem. Biol. Drug Des.*, **94(1)**: 1390-1401 (2019**)**.

[32] Daina A., Michielin O. Zoete V., Swiss ADME: A Free Web Tool to Evaluate Pharmacokinetics, Drug-Likeness and Medicinal Chemistry Friendliness of Small Molecules, *Scientific Reports*, **7(1)**: 42717 (2017**)**.

[33] Xiong G., Wu Z., Yi J., Fu L., Yang Z., Hsieh C., Yin M., Zeng X., Wu C., Lu A., Chen X., Hou T. Cao D., ADMETlab 2.0: An Integrated Online Platform for Accurate and Comprehensive Predictions of ADMET Properties, *Nucleic Acids Research*, **49(W1)**: p. W5-W14 (2021**)**.

[34] Molsoft L., Drug-Likeness and Molecular Property Prediction. (2018).

[35] Banerjee P., Eckert A.O., Schrey A.K. Preissner R., ProTox-II: A Webserver for the Prediction of Toxicity of Chemicals, *Nucleic Acids Research*, **46(W1)**: W257-W263 (2018**)**.

[36] Banerjee P., Dunkel M., Kemmler E. Preissner R., SuperCYPsPred-a Web Server for the Prediction of Cytochrome Activity, *Nucleic Acids Res*, **48(W1)**: W580-w585 (2020**)**.

[37] Daina A., Zoete V., A BOILED-Egg To Predict Gastrointestinal Absorption and Brain Penetration of Small Molecules, *Chem. Med. Chem.*, **11(11)**: p. 1117-1121 (2016**)**.

[38] de Freitas L.V., Da Silva C.C.P., Ellena J., Costa L.A.S., Rey N.A., Structural and Vibrational Study of 8-Hydroxyquinoline-2-Carboxaldehyde Isonicotinoyl Hydrazone – A Potential Metal–Protein Attenuating Compound (MPAC) for the Treatment of Alzheimer's Disease, *Spectrochimica Acta Part A: Molecular and Biomolecular Spectroscopy*, **116**: p. 41-48 (2013**)**.

[39] Szklarzewicz J., Jurowska A., Matoga D., Kruczała K., Kazek G., Mordyl B., Sapa J. Papież M., Synthesis, Coordination Properties and Biological Activity of Vanadium Complexes with Hydrazone Schiff Base Ligands, *Polyhedron*, **185**: 114589 (2020**)**.

[40] Arabahmadi R., Hydrazone-Based Schiff Base Dual Chemosensor for Recognition of Cu2+ and F− by 1:2 Demultiplexer, Half Adder, Half Subtractor, Molecular Keypad Lock and Logically Reversible Transfer Gate Logic Circuits and its Application as Test Kit, *Journal of Photochemistry and Photobiology A: Chemistry*, **427**: 113797 (2022**)**.

[41] Jassem A.M., Hassan Q.M.A., Almashal F.A., Sultan H.A., Dhumad A.M., Emshary C.A., Tuma Albaaj L.T., Spectroscopic Study, Theoretical Calculations, and Optical Nonlinear Properties of Amino Acid (Glycine)-4-Nitro Benzaldeyhyde-Derived Schiff Base, *Optical Materials*, **122**: 111750 (2021**)**.

[42] Shankar M., Dennis Raj A., Jeeva M., Purusothaman R., Vimalan M., Vetha Potheher I., Synthesis, Crystal Growth, Thermal and Laser Damage Threshold Properties of New Schiff Base NLO Material 4-Nitro-Benzoic Acid (3-Ethoxy-2-Hydroxy-Benzylidene)-Hydrazide, *Materials Letters*, **232**: p. 113-117 (2018**)**.

[43] Parvarinezhad S., Salehi M., Synthesis, Characterization, Crystal Structures, Hirshfeld Surface Analysis and DFT Computational Studies of New Schiff Bases Derived from Phenylhydrazine, *Journal of Molecular Structure*, **1222**: 128780 (2020**)**.

[44] Warad I., Suboh H., Al-Zaqri N., Alsalme A., Alharthi F.A., Aljohani M.M., Zarrouk A., Synthesis and Physicochemical, DFT, Thermal and DNA-Binding Analysis of a New Pentadentate N3S2 Schiff Base Ligand and its $[CuN_3S_2]^{2+}$ Complexes, *RSC Advances*, **10(37)**: 21806-21821 (2020**)**.

[45] Raghi K.R., Sherin D.R., Saumya M.J., Arun P.S., Sobha V.N., Manojkumar T.K., Computational Study of Molecular Electrostatic Potential, Docking and Dynamics Simulations of Gallic Acid Derivatives as ABL Inhibitors, *Computational Biology and Chemistry*, **74**: 239-246 (2018**)**.

[46] Sivakumar C., Balachandran V., Narayana B., Salian V.V., Revathi B., Shanmugapriya N., Vanasundari K., Molecular Spectroscopic Assembly of 3-(4-Chlorophenyl)-5-[4-(Propane-2-yl) Phenyl] 4, 5-Dihydro-1H Pyrazole-1-Carbothioamide, Antimicrobial Potential and Molecular Docking Analysis, *Journal of Molecular Structure*, **1210**: 128005 (2020**)**.

[47] Mumit M.A., Pal T.K., Alam M.A., Islam M.A.-A.-A.-A., Paul S., Sheikh M.C., DFT Studies on Vibrational and Electronic Spectra, HOMO–LUMO, MEP, HOMA, NBO and Molecular Docking Analysis of Benzyl-3-N-(2,4,5-Trimethoxyphenylmethylene) Hydrazinecarbodithioate, *Journal of Molecular Structure*, **1220**: 128715 (2020**)**.

[48] Mohammed K., Mohammed A.A.K., Abdel Hakiem A.F., Mahfouz R.M., Computational Evaluation on the Molecular Conformation, Vibrational Spectroscopy, NBO Analysis and Molecular Docking of Betaxolol and Betaxolol-Chlorthalidone Cocrystals, *Journal of Molecular Structure*, **1209**: 127744 (2020**)**.

[49] Şahin S., Dege N., Synthesis, Characterization, X-ray, HOMO-LUMO, MEP, FT-IR, NLO, Hirshfeld Surface, ADMET, Boiled-Egg Model Properties and Molecular Docking Studies with Human Cyclophilin D (CypD) of a Schiff Base Compound: (E)-1-(5-Nitro-2-(Piperidin-1-yl)Phenyl)-N-(3-Nitrophenyl)Methanimine, *Polyhedron*, **205**: 115320 (2021**)**.

[50] Uludağ N., Serdaroğlu G., An Improved Synthesis, Spectroscopic (FT-IR, NMR) Study and DFT Computational Analysis (IR, NMR, UV–Vis, MEP Diagrams, NBO, NLO, FMO) of the 1,5-Methanoazocino[4,3-b]Indole Core Structure, *Journal of Molecular Structure*, **1155**: 548-560 (2018**)**.

[51] Suresh S., Gunasekaran S., Srinivasan S., Vibrational Spectra (FT-IR, FT-Raman), Frontier Molecular Orbital, First Hyperpolarizability, NBO Analysis and Thermodynamics Properties of Piroxicam by HF and DFT Methods, *Spectrochimica Acta Part A: Molecular and Biomolecular Spectroscopy*, **138**: p. 447-459 (2015**)**.

[52] Hassan S.A., Abdullah M.N., Aziz D.M., An Efficient One-Pot Three-Component Synthesis, Molecular Docking, ADME and DFT Predictions of New Series Thiazolidin-4-one Derivatives Bearing a Sulfonamide Moiety as Potential Antimicrobial and Antioxidant Agents, *Egyptian Journal of Chemistry*, **65(8)**: 133-146 (2022**)**.

[53] Khalid M., Ali A., Haq S., Tahir M.N., Iqbal J., Braga, A.A.C., Ashfaq M., Akhtar S.U.H., O-4-Acetylamino-Benzenesulfonylated Pyrimidine Derivatives: Synthesis, SC-XRD, DFT Analysis and Electronic Behaviour Investigation, *Journal of Molecular Structure*, **1224**: p. 129308 (2021**)**.

[54] Şahin S., Dege N., A Newly Synthesized Small Molecule: The Evaluation Against Alzheimer's Disease by in Silico Drug Design and Computational Structure Analysis Methods, *Journal of Molecular Structure*, **1236**: 130337 (2021**)**.

[55] Şahin S., Dege N., (E)-N-(3-Chlorophenyl)-1-(5-Nitro-2-(Piperidin-1-yl)Phenyl)Methanimine: X-Ray, DFT, ADMET, Boiled-Egg Model, Druggability, Bioavailabilty, and Human Cyclophilin D (CypD) Inhibitory Activity, *Journal of Molecular Structure*, 131744 (2021**)**.

[56] Soliman S.M., Hagar M., Ibid F., El Ashry E.S.H., Experimental and Theoretical Spectroscopic Studies, HOMO–LUMO, NBO Analyses and Thione–Thiol Tautomerism of a New Hybrid of 1,3,4-Oxadiazole-Thione with Quinazolin-4-One, *Spectrochimica Acta Part A: Molecular and Biomolecular Spectroscopy*, **145**: 270-279 (2015).

[57] Fan J., de Lannoy I.A.M., Pharmacokinetics, *Biochemical Pharmacology*, **87(1)**: 93-120 (2014**)**.

[58] McDonnell A.M., Dang C.H., Basic Review of the Cytochrome p450 System, *Journal of the Advanced Practitioner in Oncology*, **4(4)**: 263-268 (2013**)**.

[59] Olsen L., Oostenbrink C., Jørgensen F.S., Prediction of Cytochrome P450 Mediated Metabolism, *Advanced Drug Delivery Reviews*, **86**: 61-71 (2015**)**.

[60] Zhao L., Sun N., Tian L., Zhao S., Sun B., Sun Y., Zhao D., Strategies for the Development of Highly Selective Cytochrome P450 Inhibitors: Several CYP Targets in Current Research, *Bioorganic & Medicinal Chemistry Letters*, **29(16)**: 2016-2024 (2019**)**.

[61] Banerjee P., Dunkel M., Kemmler E., Preissner R., SuperCYPsPred—A Web Server for the Prediction of Cytochrome Activity, *Nucleic Acids Research*, **48(W1)**: W580-W585 (2020**)**.

[62] David S., Hamilton J.P., Drug-Induced Liver Injury, *US Gastroenterol Hepatol Rev*, **6**: p. 73-80 (2010**)**.

[63] Honma M., An Assessment of Mutagenicity of Chemical Substances by (Quantitative) Structure–Activity Relationship, *Genes and Environment*, **42(1)**: 23 (2020**)**.

[64] Benigni R., Bossa C., Mechanisms of Chemical Carcinogenicity and Mutagenicity: A Review with Implications for Predictive Toxicology, *Chemical Reviews*, **111(4)**: 2507-2536 (2011**)**.

[65] Richard A.M., Huang R., Waidyanatha S., Shinn P., Collins B.J., Thillainadarajah I., Grulke C.M., Williams A.J., Lougee R.R., Judson R.S., Houck K.A., Shobair M., Yang C., Rathman J.F., Yasgar A., Fitzpatrick S.C., Simeonov A., Thomas R.S., Crofton K.M., Paules R.S., Bucher J.R., Austin C.P., Kavlock R.J., Tice R.R., The Tox21 10K Compound Library: Collaborative Chemistry Advancing Toxicology, *Chemical Research in Toxicology*, **34(2)**: 189-216 (2021**)**.

[66] Huang R., Xia M., Nguyen D.-T., Zhao T., Sakamuru S., Zhao J., Shahane S.A., Rossoshek A., Simeonov A., Tox21Challenge to Build Predictive Models of Nuclear Receptor and Stress Response Pathways as Mediated by Exposure to Environmental Chemicals and Drugs, *Frontiers in Environmental Science*, **3(85)** (2016**)**.